# Study of the Proton Single-Particle Strengths in 19F and Proton Shell Closure of 180 through the 180(d, n)19F Reaction

| | |
|---|---|
| 著者 | Terakawa A., Tohei T., Nakagawa T., Takamatsu J., Narita A., Hosomi K., Orihara H., Ishii K., Niizeki T., Ohura M., Hosaka M., Jon G. C., Miura K., Ohnuma H. |
| journal or publication title | CYRIC annual report |
| volume | 1991 |
| page range | 12-20 |
| year | 1991 |
| URL | http://hdl.handle.net/10097/49624 |

# I. 3. Study of the Proton Single-particle Strengths in $^{19}F$ and Proton Shell Closure of $^{18}O$ through the $^{18}O(d, n)^{19}F$ Reaction

*Terakawa A., Tohei T., Nakagawa T., Takamatsu J., Narita A., Hosomi K., Orihara H.*, Ishii K.*, Niizeki T.****, Ohura M.**, Hosaka M.*, Jon G.C.*, Miura K.*** and Ohnuma H.*****

*Department of Physics, Faculty of Science, Tohoku University ]*
*Cyclotron and Radioisotope Center, Tohoku University**
*The Institute of Physical and Chemical Research ( RIKEN )** Tohoku Institute of Technology****
*Department of Physics, Tokyo Institute of Technology*****

An interesting aspect of $^{19}F$ is the strong fragmentation [1,2] of the proton single-particle strength compared with the case of $^{17}F$ which shows the considerable single-particle character in the low lying states. The fragmentation in $^{19}F$ is related to the configuration mixing of the initial and/or final states due to the addition of two neutrons. The spectroscopic information for $^{19}F$ reported in the previous works [1,2] has been limited in the proton bound state region of $E_x < 8$ MeV, while the recent shell model [3] in the basis of the complete 2s1d shell model space predicts the location of the large amount of the 2s1d strengths in the higher excitation region.

In this report, we present a systematic study of the $^{18}O(d, n)^{19}F$ reaction at $E_d = 25$ MeV. Since we have investigated the spectroscopic strengths up to $E_x = 15$ MeV which corresponds to about 1 in this mass region, most valence strengths of the 2s1d shell will be covered in the present measurement. Hence, we aim to test the complete 2s1d shell model wave functions from the comparison between the experimental results and the theoretical predictions.

As is well known [4], the sum of the spectroscopic strengths for a quantum number n j gives the occupancy of the shell model orbit in the target ground state. In the simple shell model consideration the 1p proton shell in the ground states of oxygen isotopes is completely occupied. However, the recent many-body theories [5,6] predict the sizable depletion of the occupation probability for the normally occupied orbits below the Fermi level due to long-range, tensor and short-range correlations. The precise determination of the occupation probability leads to the understanding of the nuclear many-body problem. We also aim to deduce the occupation probabilities of the proton orbits in the ground states of oxygen isotopes in the framework of the combined analysis [7] of the stripping and pick-up data on the same target nucleus.

The experiment was performed at the Cyclotron and Radioisotope Center ( CYRIC ), Tohoku University. The experimental procedure has been described in the last annual report [8]. A typical excitation energy spectrum is shown in Fig. 1. Overall energy resolution was 185 keV ( FWHM ) for the neutrons leading to the low lying states in the residual nucleus. Backgrounds are due to neutrons mainly from the platinum windows. Structureless backgrounds have been observed in empty runs. Errors in the absolute magnitudes of the cross sections are estimated to be less than 15 %.

Angular distributions for each transferred are shown in Figs. 2 and 3 together with the results of the zero-range adiabatic deuteron breakup approximation (ADBA) calculations [9], where s-wave deuteron breakup effects have been included. The calculations have been performed with the code DWUCK4 [10]. The potentials used in the calculation have been described in ref. 8). Spectroscopic results for $^{19}$F are summarized in Table 1. The spins and parities [11] of the final states needed in the present calculation have been established in most cases. The observed transitions have exhausted almost the whole strength for the sum rule limit over the 2s1d shell.

The strength distributions for each 2s1d shell orbit are illustrated in Fig. 4 together with the predictions [3] by the complete 2s1d shell model. The shell model calculations were performed with the shell model code OXBASH [12]. The comparisons between the experimental results and the shell model predictions shows that the $1d_{5/2}$ strength distribution is successfully reproduced by the theory, while the agreement is quite poor in the cases of the $2s_{1/2}$ and $1d_{3/2}$ strengths. The discrepancies may indicate more complicated configuration mixing in the final states than that predicted by the shell model; since $^{19}$F has well-known low lying 4 particle - 1 hole states ( mainly $(1p)^{-1}(2s1d)^4$ configurations), such as the 0.110 MeV, $1/2^-$ and 1.459 MeV, $3/2^-$ states, it is plausible that the high lying states have the mixed configurations including the components of the excited $^{16}$O core, which have not been taken into account in the 2s1d shell model calculation [3]. Therefore, we conclude that the discrepancies in both results suggest the necessity of the detailed shell model calculation with more extended model space for this mass region.

The sum of the spectroscopic strengths over all the final states for each quantum number n j are related to the target ground state population through the sum rule by French and Macfarlane [4]. However, the influence from the uncertainties in the DWBA treatment may make the application of the sum rule unreliable; the cross section is quite sensitive to both optical potentials and assumed geometry for the bound potential. In order to avoid this difficulty in the determination of the occupation probability, the combined analysis of the stripping and pick-up data on the same target nucleus has been proposed [7].

We performed the combined analysis of the present data and those of the $^{18}$O(d, $^3$He)$^{17}$N reaction at $E_d$ = 52 MeV [13] for deducing the occupation probabilities and single-particle energies in the target ground state. The result of the analysis is given in Table 2 together with that for $^{16}$O using the $^{16}$O(d, n)$^{17}$F data at $E_d$ = 25 MeV [14] and the $^{16}$O(d,

$^{3}$He)$^{15}$N data at $E_d$ = 34.4 MeV [15]. The deduced ground state properties of $^{16,18}$O have been interpreted in terms of the BCS theory. Figure 5 shows the distributions of the occupation probabilities and the results of the least squares fit of the BCS function to the data. The obtained Fermi ($\lambda$) and gap ($\Delta$) energies are;

$\lambda$ = - 6.0 MeV, $\Delta$ = 2.0 MeV for $^{16}$O and $\lambda$ = - 9.1 MeV, $\Delta$ = 2.3 MeV for $^{18}$O, indicating increases in both the Fermi energy in its magnitude and the effect of paring correlation for $^{18}$O. It is concluded that the depletion of the Fermi sea in the ground states of oxygen isotopes increases in going from the doubly magic nucleus $^{16}$O to $^{18}$O because of the rearrangement of the proton shell through configuration mixing by the addition of two neutrons.

In summary, a systematic study of the $^{18}$O(d, n)$^{19}$F reaction at $E_d$ = 25 MeV was made. The spectroscopic strengths up to $E_x$ = 15 MeV were obtained from the ADBA calculations. The observed transitions have exhausted almost the whole strength for the sum rule limit over the 2s1d shell. The comparison between the experimental results and the predictions [3] by the recent 2s1d shell model shows the discrepancies in the distributions of the $2s_{1/2}$ and $1d_{3/2}$ strengths. The occupation probabilities and single-particle energies of the proton shell in the ground states of $^{16,18}$O were deduced from the combined analysis of the stripping and pick-up data on the same target nucleus. The result of the analysis leads to a reasonable conclusion that the depletion of the Fermi sea in $^{18}$O is larger than that in $^{16}$O.

## References


1) Green L. L. et al, Nucl. Phys. **A142** (1970) 137.
2) Schmidt C. and Duhm H. H., Nucl. Phys. **A155** (1970) 644.
3) Wildenthal B. H., Progress in particle and nuclear physics, vol. 11(Pergamon, New York 1983) p.5.
4) French J. B. and Macfarlane M. H., Nucl. Phys. **26** (1961) 168. 5), Pandharipande V. R. et al., Phys. Rev. Lett. **53** (1984) 1133 6) and Jaminon M. et al., Nucl. Phys. **A473** (1987) 509.
7) Pfeiffer A. et al., Nucl. Phys. **A247** (1986) 168.
8) Terakawa A. et al., CYRIC Annual Report (1990) p.5.
9) Wales G. L. and Johnson R. C., Nucl. Phys. **A247** (1976) 168.
10) Kunz P. D., The code DWUCK4, unpublished.
11) Ajzenberg-Selove F., Nucl. Phys. **A475** (1987) 1.
12) Brown B. A. et al., The shell model code OXBASH, unpublished.
13) Mairl G., et al., Nucl. Phys. **A280** (1977) 97.
14) Kawamura T., Ph. D. thesis, Tohoku University (1986).
15) Hiebert J. C. et al., Phys. Rev. **154** (1967) 898.

Table 1. Experimental spectroscopic strengths in $^{19}$F.

| $E_x$(MeV)[Ref.11] | $J^\pi$ ; T[Ref.11] | (d,n), $E_d$=25 MeV $E_x$(MeV) | $\ell$ | n$\ell$j | $(2J_f+1)C^2S$ | ($^3$He,d), $E_d$=11 MeV[Ref.1] $\ell$ | n$\ell$j | $(2J_f+1)C^2S$ | ($^3$He,d), $E_d$=16 MeV[Ref.2] $\ell$ | n$\ell$j | $(2J_f+1)C^2S$ |
|---|---|---|---|---|---|---|---|---|---|---|---|
| g.s. | $1/2^+$ | g.s. | 0 | $2s_{1/2}$ | 0.50 | 0 | $2s_{1/2}$ | 0.6 | 0 | $2s_{1/2}$ | 0.42 |
| 0.110 | $1/2^-$ | | | | | 1 | $1p_{1/2}$ | 0.24 | 1 | $1p_{1/2}$ | 0.224 |
| 0.197 | $5/2^+$ | 0.20 | 2 | $1d_{5/2}$ | 2.59 | 2 | $1d_{5/2}$ | 2.55 | 2 | $1d_{5/2}$ | 2.45 |
| 1.459 | $3/2^-$ | | | | | 1 | $1p_{3/2}$ | 0.144 | 1 | $1p_{3/2}$ | 0.098 |
| 1.554 | $3/2^+$ | 1.55 | 2 | $1d_{3/2}$ | 1.15 | 2 | $1d_{3/2}$ | 1.17 | 2 | $1d_{3/2}$ | 1.01 |
| 4.550 | $5/2^+$ | 4.55 | 2 | $1d_{5/2}$ | 0.46 | | | | | | |
| 5.535 | $5/2^+$ | 5.54 | 2 | $1d_{5/2}$ | 0.21 | (3) | $1f_{7/2}$ | 0.29 | 2 | $1d_{3/2}$ | 0.31 |
| 6.088 | $3/2^-$ | 6.09 | 1 | $2p_{3/2}$ | 0.17 | 1 | $2p_{1/2}$ | 0.426 | 1 | $2p_{1/2}$ | 0.12 |
| 6.255 | $1/2^+$ | 6.26 | 0 | $2s_{1/2}$ | 0.31 | 0 | $2s_{1/2}$ | 0.41 | 0 | $2s_{1/2}$ | 0.19 |
| 6.497 | $3/2^+$ | 6.50 | 2 | $1d_{3/2}$ | 0.15 | 2 | $1d_{3/2}$ | 0.133 | | | |
| 6.787 | $3/2^-$ | 6.79 | 1 | $2p_{3/2}$ | 0.13 | 1 | $2p_{3/2}$ | 0.29 | 1 | $2p_{3/2}$ | 0.17 |
| 6.927 | $7/2^-$ | 6.93 | 3 | $1f_{7/2}$ | 0.50 | | | | 3 | $1f_{7/2}$ | 0.385 |
| | | 7.11 | 2 | $1d_{5/2}$ | 0.21 | 2 | $1d_{5/2}$ | 0.52 | 2 | $1d_{5/2}$ | 0.087 |
| 7.540 | $5/2^+;3/2$ | 7.54 | 1 | $1d_{5/2}$ | 1.54 | 2 | $1d_{5/2}$ | 0.82 | 2 | $1d_{5/2}$ | 0.665 |
| 8.015 | $5/2^+$ | 8.06 | 0+2 | $1d_{5/2}$ | 0.44 | | | | | | |
| 8.137 | $1/2^+$ | 8.06 | 0+2 | $2s_{1/2}$ | 0.23 | | | | | | |
| | | 8.30 | 2 | $1d_{5/2}$ | 0.16 | | | | | | |
| 8.589 | $3/2^-$ | 8.59 | 1 | $2p_{3/2}$ | 0.17 | | | | | | |
| 8.793 | $1/2^+;3/2$ | 8.79 | 0 | $2s_{1/2}$ | 0.52 | | | | | | |
| 9.204 | $3/2^+$ | 9.14 | 2 | $1d_{3/2}$ | 0.10 | | | | | | |
| 9.668 | $3/2^+$ | 9.67 | 2 | $1d_{3/2}$ | 0.44 | | | | | | |
| 10.308 | $3/2^+$ | 10.31 | 2 | $1d_{3/2}$ | 0.49 | | | | | | |
| 10.555 | $3/2^+;3/2$ | 10.56 | 2 | $1d_{3/2}$ | 0.24 | | | | | | |
| | | 10.88 | 2 | $1d_{3/2}$ | 0.21 | | | | | | |
| | | 11.02 | 2 | $1d_{3/2}$ | 0.15 | | | | | | |
| 11.540 | $5/2^+$ | 11.55 | 2 | $1d_{5/2}$ | 0.13 | | | | | | |
| 11.652 | $3/2^+;3/2$ | 11.74 | 2 | $1d_{3/2}$ | 0.20 | | | | | | |
| 12.221 | $3/2^+$ | 12.22 | 2 | $1d_{3/2}$ | 0.24 | | | | | | |
| 12.86 | $3/2^+;3/2$ | 12.86 | 2 | $1d_{3/2}$ | 0.39 | | | | | | |
| 13.317 | $7/2^-;3/2$ | 13.34 | 3 | $1f_{3/2}$ | 0.24 | | | | | | |
| 13.731 | $7/2^-;3/2$ | 13.75 | 3 | $1f_{3/2}$ | 0.23 | | | | | | |

Table 2. Occupation probabilities and single-particle energies in $^{16,18}O$.

| | $^{16}O$ | | $^{18}O$ | |
|---|---|---|---|---|
| Proton orbit | Energy (MeV) | Occupation probability | Energy (MeV) | Occupation probability |
| $1p_{3/2}$ | −18.5 | 0.96 | −21.5 | 0.95 |
| $1p_{1/2}$ | −11.6 | 1.00 | −15.3 | 1.03 |
| $1d_{5/2}$ | −1.5 | 0.05 | −7.8 | 0.14 |
| $2s_{1/2}$ | −0.5 | 0.06 | −6.3 | 0.15 |

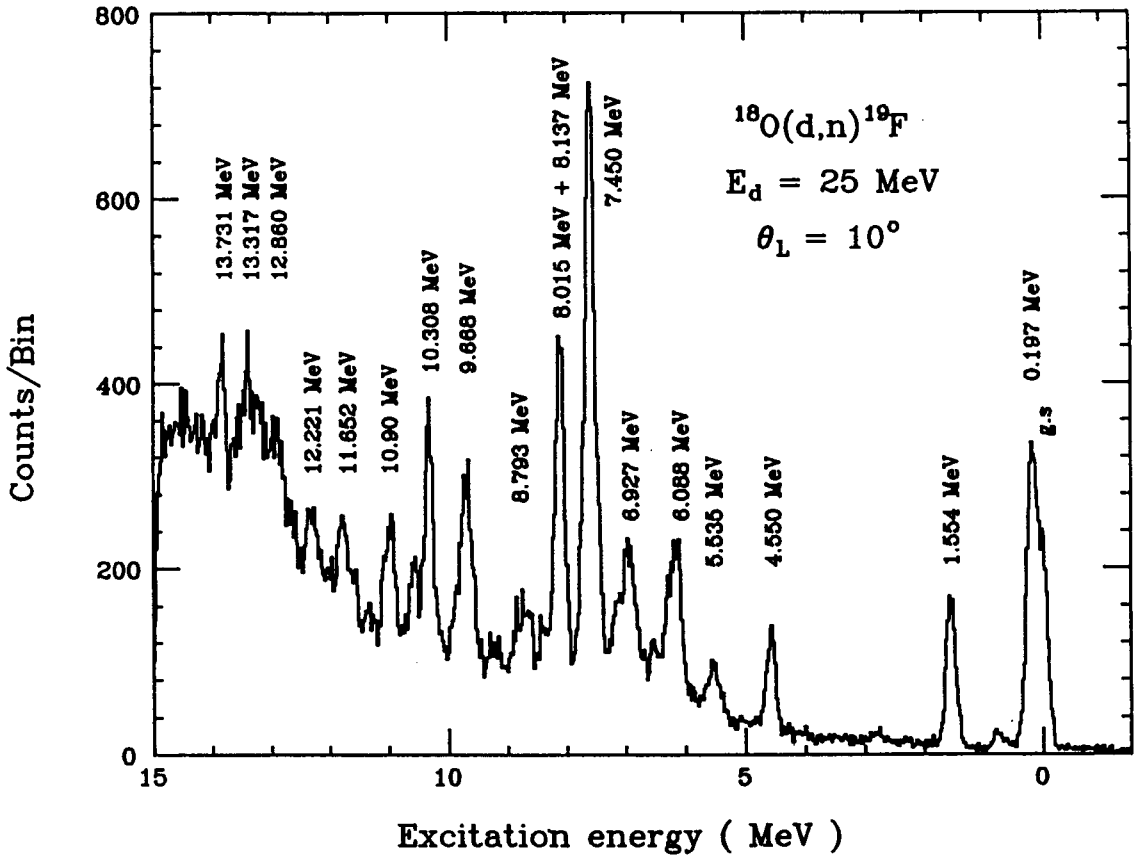


Fig. 1. Energy spectrum of the $^{18}O(d, n)^{19}F$ reaction at $\theta_L = 10^o$.

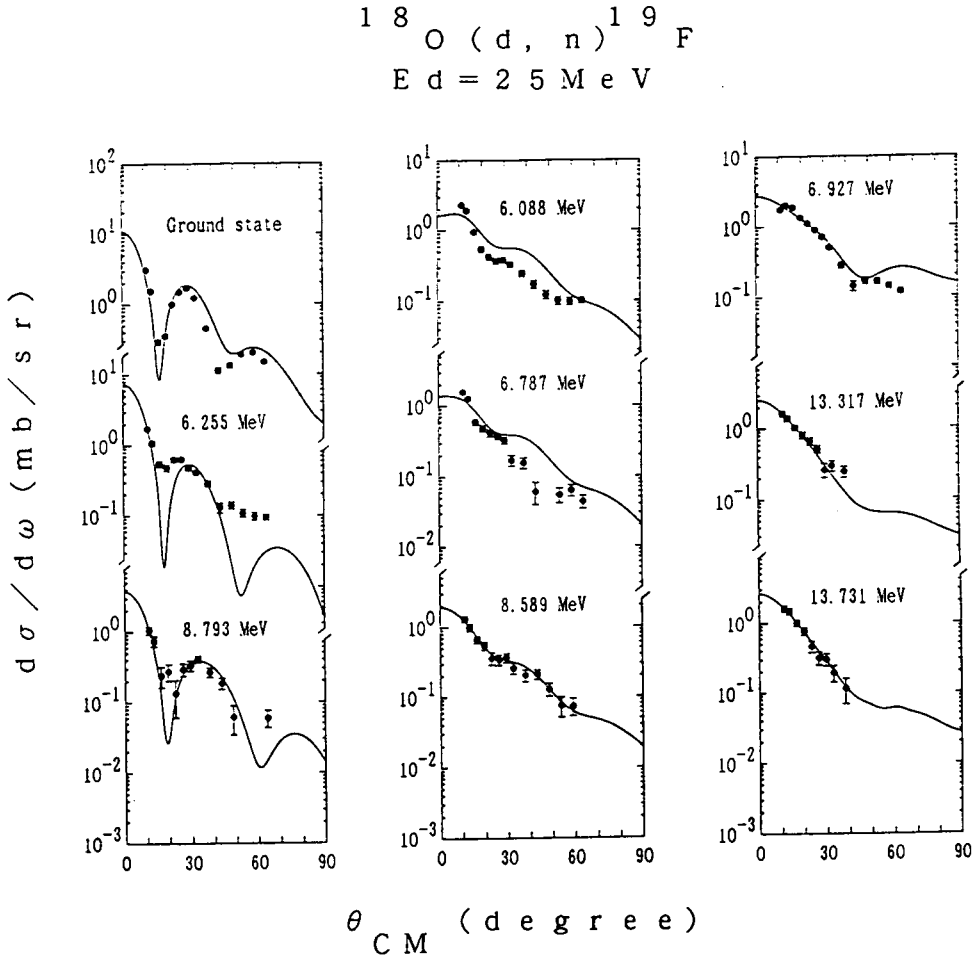


Fig. 2. Angular distributions of the differential cross sections for the transferred $\ell = 0$, 1 and 3. The solid lines represent the results of the ADBA calculations.

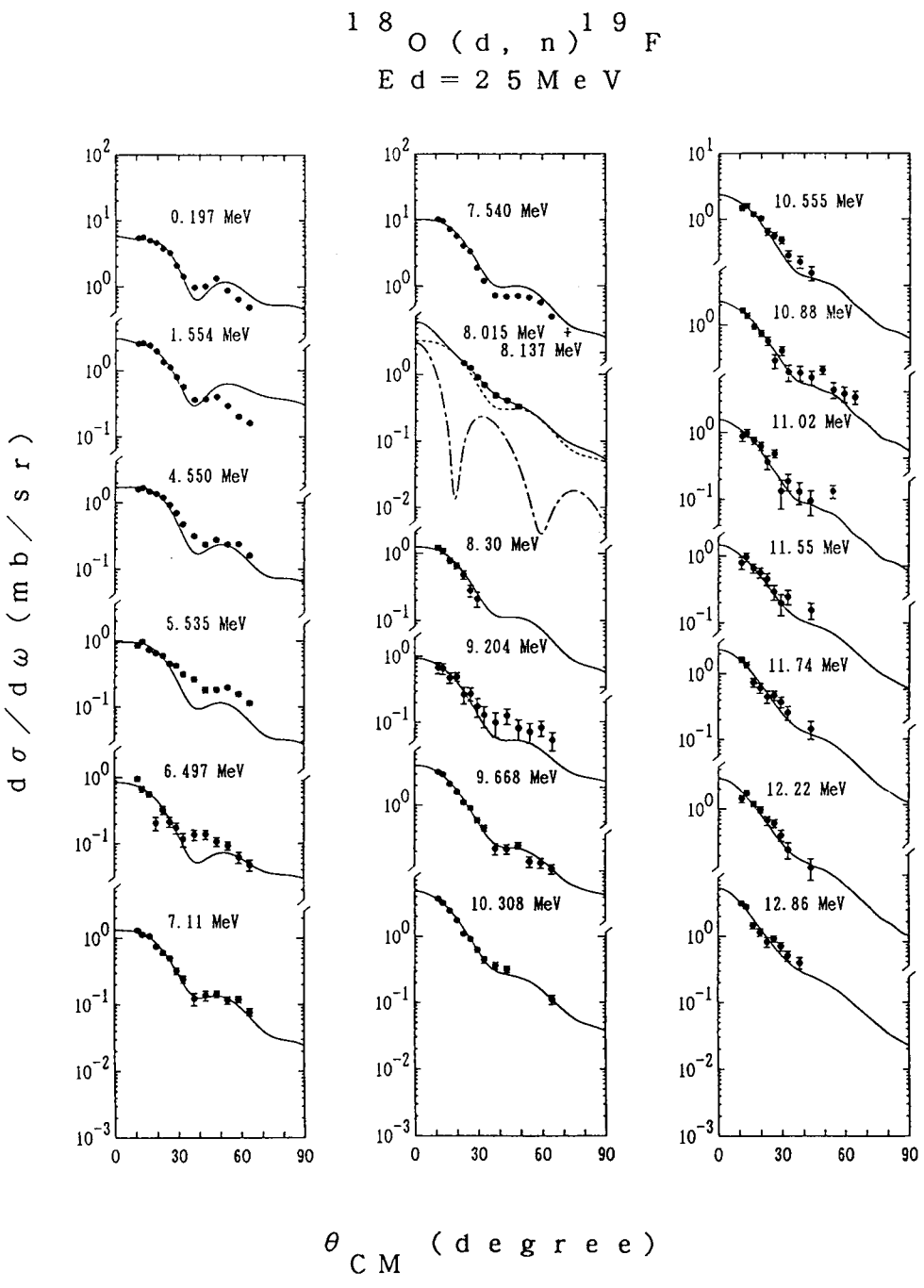


Fig. 3. Angular distributions of the differential cross sections for the transferred $\ell = 2$. Thesolid lines represent the results of the ADBA calculations. In the case of the doublet peak of the 8.015 MeV, 5/2+ state and the 8.137 MeV, 1/2+ state, the solid line indicates the sum of the decomposed $\ell = 2$ (dashed line ) and $\ell = 0$ (solid-dashed line ) contributions.

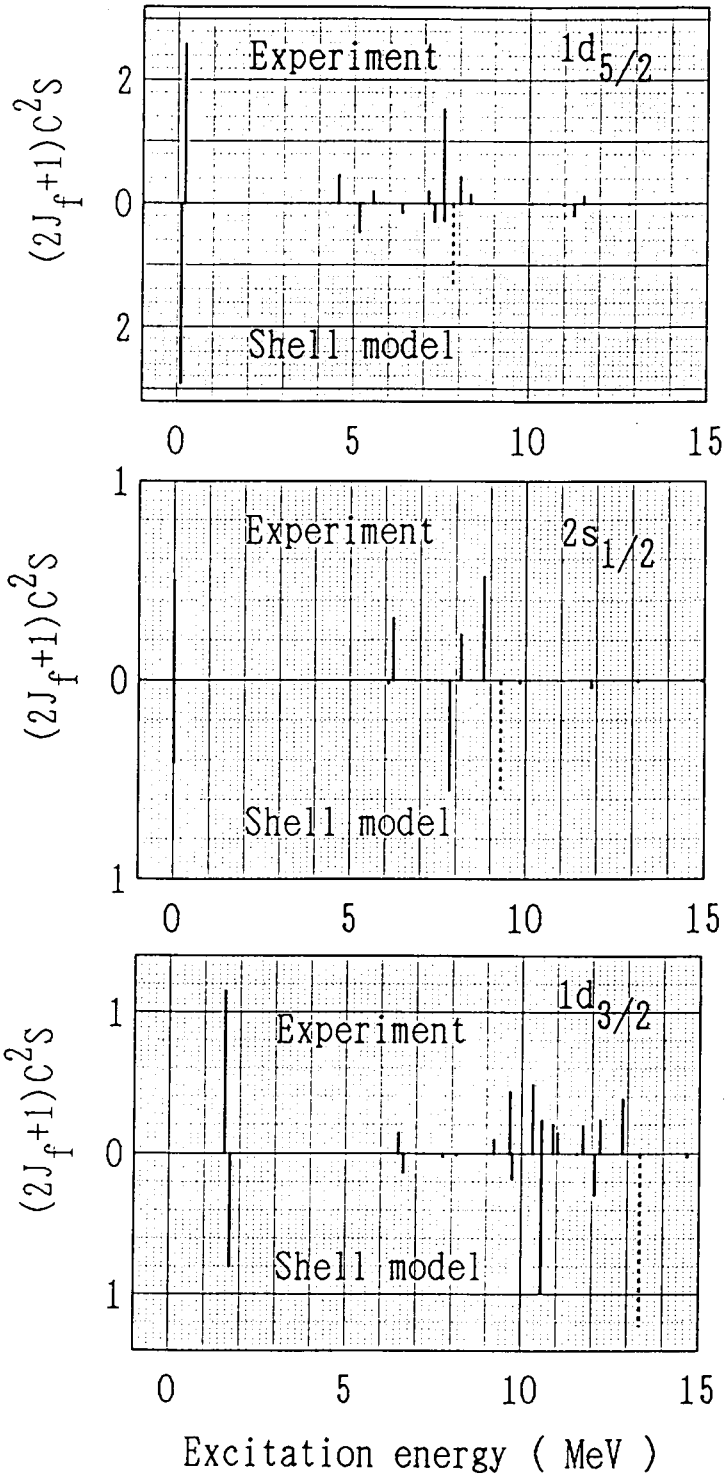


Fig. 4. Comparisons of the strength distributions for the 2s1d orbits between the experimental results and the shell model predictions. The dotted lines for the predictions indicate the distributions of the $T_>$ strength.

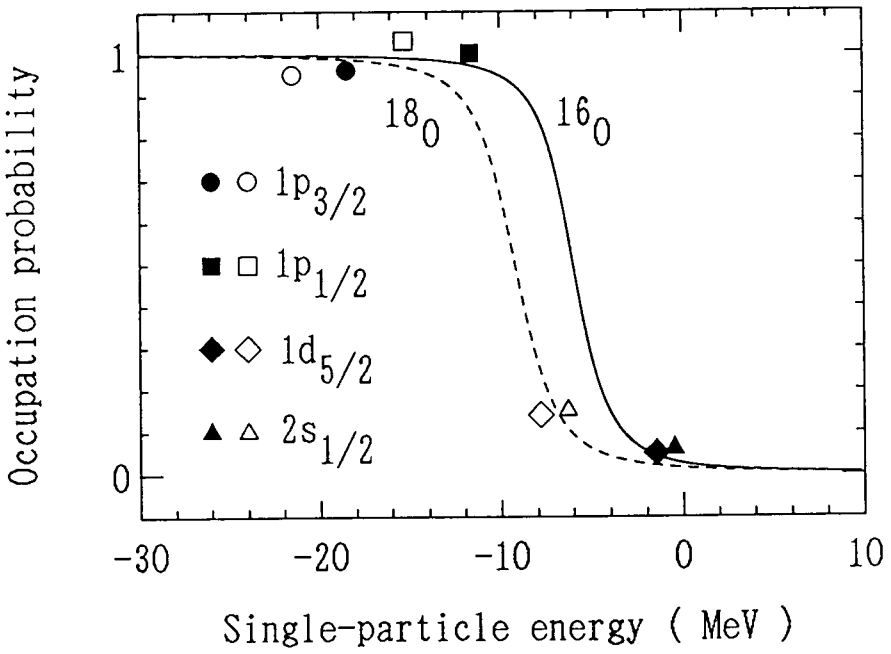


Fig. 5. Distributions of the occupation probabilities of the proton shell in the ground states of $^{16,18}O$. Full (Open) circle, square, diamond and triangle represent the deduced occupation probabilities of the $1p_{3/2}$, $1p_{1/2}$, $1d_{5/2}$ and $2s_{1/2}$ orbits for $^{16}O$ ($^{18}O$), respectively. The solid and dashed lines indicate the results of the least squares fit of the BCS function to the data for $^{16}O$ and $^{18}O$, respectively.